TECHNISCHE MECHANIK, Band 20, Heft 3, (2000), 251–264
Manuskripteingang: 24. Juli 2000

Preasymptotic Performance of Modified Mixed Finite Element Schemes for Plates

K. Weinberg

This paper is devoted to numerical investigations on shear–locking free finite element methods for Reißner–Mindlin plates recently introduced in mathematical literature. We verify and improve theoretically predicted convergence rates and provide a technique to handle preasymptotic instabilities. The approximation of stress resultants is monitored by benchmark computation. Moreover we give experimental evidence that a new adaptive automatic mesh-refining algorithm yield superior approximations. Summarizing our comprehensive numerical studies by some typical examples we deduce recommendations for employing the modified mixed finite element schemes in engineering practice.

1 Introduction

The Reißner-Mindlin equations of the moderately thick plate

$$\frac{t^2}{6}\,\mathrm{div}\left(\frac{\nu}{1-\nu}\,\mathcal{I}\,\mathrm{div}\,\vartheta+\varepsilon(\vartheta)\right)+(\nabla w-\vartheta)=0 \tag{1}$$

$$\mathrm{div}(\nabla w-\vartheta)+kf=0 \tag{2}$$

for the vertical displacement w and the rotations of the plate normal ϑ are frequently applied and well-analyzed. Using the standard variational form of (1)–(2) the finite element approximation deteriorates as the plate thickness t becomes small, known as shear locking. A standard technique to handle such parameter dependent problems is passing to a mixed variational form. This in general requires deeper mathematical analysis as an arbitrary choice of discrete ansatz and test spaces yields instabilities.

Very recently, new finite element technologies for an effective numerical treatment of the plate problem were introduced in the mathematical literature (Arnold and Brezzi, 1993; Brezzi and Fortin, 1991; Lovadina, 1996; Boffi et al., 1997; Chapelle and Stenberg, 1998). But these finite element schemes partially show a strange preasymptotic performance, which rather suggests errors in our code than the theoretically predicted convergence rates, Figure 1. This rises the question wether the mathematical predictions, which are true for small mesh sizes $h \to 0$, are observed for reasonable sized (but for the mathematical analysis possibly too coarse) meshes, too.

The aim of this paper is to present our numerical experience with modified mixed finite element methods for Reißner–Mindlin plates. Thus we first provide in Section 2 detailed notation, weak and discrete formulation and different approximation schemes. A technique to avoid instabilities of finite element computation even in the preasymptotic range is presented in Section 3. We discuss the question of how to estimate the error of discretization in Section 4, followed in Section 5 by an automatic adaptive mesh–refining algorithm. In Section 6 we compare the convergence behaviour of different finite element schemes by some typical examples applying uniform and adaptive mesh refinements. In Section 7 we summarize our numerical studies on approximation quality of stresses and stress resultants.

As a result we can establish that all presented finite element schemes can be employed in engineering practice using a simple stabilisation technique. We point out the superiority of a $P_2-P_2-P_0$ discretisation with mesh adapted stabilisation parameter α in practical computations.

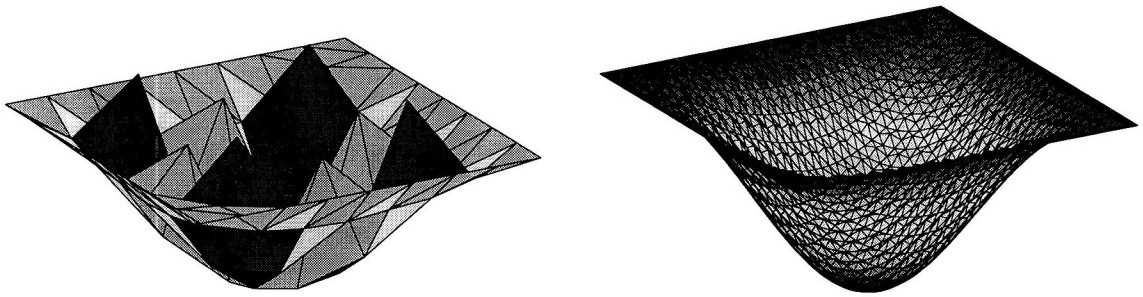

Figure 1: Quadratic plate under uniform load: displacement function computed with $\alpha = 1$

2 Mixed Formulation and Finite Element Discretisation

Following Arnold and Brezzi (Arnold and Brezzi, 1993) we introduce a shear variable γ.

$$\gamma := (t^{-2} - \alpha)(\nabla w - \vartheta) \tag{3}$$

The weak form of the Reißner-Mindlin plate model is rewritten with bilinear forms

$$a(\vartheta, w; \varphi, v) := \int_\Omega \varepsilon(\vartheta) : \mathcal{C}\varepsilon(\varphi)\, dx + \int_\Omega \alpha\,(\vartheta - \nabla w)\cdot(\varphi - \nabla v)\, dx \tag{4}$$

$$b(\vartheta, w; \eta) := \int_\Omega (\vartheta - \nabla w)\cdot \eta\, dx \tag{5}$$

$$c(\gamma; \eta) := \int_\Omega \beta\,\gamma\cdot\eta\, dx \tag{6}$$

for plate domain $\Omega \subset \mathbb{R}^2$, $\vartheta, \varphi \in H_0^1(\Omega)^2$, $v, w \in H_0^1(\Omega)$, and $\gamma, \eta \in L^2(\Omega)^2$. Here and below, $f \in L^2(\Omega)$ is an applied force (f is already scaled by a factor $Et^3/(2k(1+\nu))$); the linear Green strain $\varepsilon(\vartheta) := \mathrm{sym} D\vartheta = (\frac{1}{2}(\partial\vartheta_j/\partial\vartheta x_k + \partial\vartheta_k/\partial\vartheta x_j))_{j,k=1,2}$ is the symmetric gradient; the elasticity operator $\mathcal{C}$ is defined by

$$\mathcal{C}\tau = \frac{1}{6k}[\tau + \frac{\nu}{1-\nu}\,\mathrm{tr}(\tau)\mathcal{I}] \tag{7}$$

where $\mathrm{tr}(\tau)$ denotes the trace of $\tau \in \mathbb{R}^{2\times 2}$ and E is Young's modulus, ν is the Poissons ratio and $k = 5/6$ the shear correction factor of the elastic plate. The critical parameter is the small thickness $t > 0$ of the plate which enters (4)-(6) through $\beta := 1/(t^{-2} - \alpha)$ where α is a parameter with $0 \le \alpha < t^{-2}$ to stabilize the discretisation. In (Arnold and Brezzi, 1993) originally α is equal 1, the classical (not modified) mixed model of (Arnold and Falk, 1989) is included for $\alpha = 0$. In this paper, the function $\alpha = \alpha(x)$ is a possibly adiscontinuous function, which may vary with $x \in \Omega$ and may be different on different finite elements. Thus the **continuous Problem** reads: *Find* $(w, \vartheta, \gamma) \in H_0^1(\Omega) \times H_0^1(\Omega)^2 \times L^2(\Omega)$ *that satisfies*

$$a(\vartheta, w; \varphi, v) + b(\varphi, v; \gamma) = \int_\Omega f v\, dx \tag{8}$$

$$b(\vartheta, w; \eta) - c(\gamma; \eta) = 0 \tag{9}$$

for all $(v, \varphi, \eta) \in H_0^1(\Omega) \times H_0^1(\Omega)^2 \times L^2(\Omega)^2$.

Here, $L^2(\Omega)$ and $H^1(\Omega)$ denote the usual Lebesgue and Sobolev spaces (Brenner and Scott, 1994) and $H_0^1(\Omega)$ is the subspace of all functions with zero boundary values with dual space $H^{-1}(\Omega)$. The mathematical analysis in (Brezzi and Fortin, 1997) shows that, in the limit $t \to 0$ and for $\alpha = 0$, the natural space for the shear variable γ is *not* $L^2(\Omega)$ but $H^{-1}(\mathrm{div}; \Omega)$ which consists of all $\gamma \in H^{-1}(\Omega)^2$ with $\mathrm{div}\,\gamma \in H^{-1}(\Omega)$ and with norms

$$\|\gamma\|_{H^{-1}(\mathrm{div};\Omega)} := \left(\|\gamma\|^2_{H^{-1}(\Omega)} + \|\mathrm{div}\,\gamma\|^2_{H^{-1}(\Omega)}\right)^{1/2} \tag{10}$$

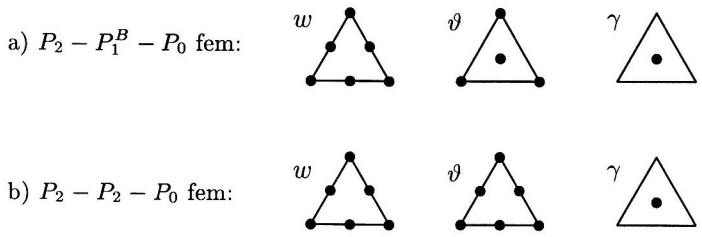

Figure 2: Finite element discretisation

$$\| \gamma \|_{H^{-1}(\mathrm{div}) \cap t \cdot L^2} := \left(\| \gamma \|^2_{H^{-1}(\mathrm{div};\Omega)} + t^2 \| \gamma \|^2_{L^2(\Omega)} \right)^{1/2} \tag{11}$$

Note, that the L^2-norm in (11) has the thickness t as a weight in order to result in a t-independent error estimation.

The finite element discretisation of (4)-(6) considers discrete subspaces $V_h \times W_h \times \Gamma_h$ of $H^1_0(\Omega) \times H^1_0(\Omega)^2 \times L^2(\Omega)$. Thus the **discrete Problem** reads: *Find* $(w_h, \vartheta_h, \gamma_h) \in V_h \times W_h \times \Gamma_h$ *that satisfies*

$$a(\vartheta_h, w_h; \phi_h, v_h) + b(\phi_h, v_h; \gamma_h) = \int_\Omega f v_h \, dx \tag{12}$$

$$b(\vartheta_h, w_h; \eta_h) - c(\gamma_h; \eta_h) = 0 \tag{13}$$

for all $(v_h, \phi_h, \eta_h) \in V_h \times W_h \times \Gamma_h$.

The discrete spaces $V_h \times W_h \times \Gamma_h$ are $\mathcal{T}$-piecewise polynomials (the index h may refer to the mesh-size of $\mathcal{T}$ but we neglect further sub-indices such as $\mathcal{T}_h$, α_h etc.) based on a regular triangulation $\mathcal{T}$ of Ω, i.e., $\mathcal{T}$ is a finite partition of Ω in closed triangles; two distinct elements T_1 and T_2 in $\mathcal{T}$ are either disjoint, or $T_1 \cap T_2$ is a complete edge E or a common node of both T_1 and T_2. The triangulation satisfies the minimum angle condition (the angles in the triangles are assumed to belong to the interval $(c_\theta, \pi - c_\theta)$ for some positive constant c_θ and so they are bounded uniformly away from 0 and π). The set of all edges in $\mathcal{T}$ is denoted as $\mathcal{E}$ and $\cup\mathcal{E}$ is the union of all edges, i.e., the skeleton of all boundaries of elements in $\mathcal{T}$. With each edge, we associate a unit normal vector n_E which coincides with the exterior normal if the edge E belongs to the boundary $\partial\Omega$. The diameter of T is denoted as h_T and the length of E is h_E. For compact notation, let $h_\mathcal{T} \in L^\infty(\Omega)$ and $h_\mathcal{E} \in L^\infty(\cup\mathcal{E})$ be given as $\mathcal{T}$- resp. $\mathcal{E}$-piecewise constant weights

$$h_\mathcal{T}|_T := h_T \quad \text{and} \quad h_\mathcal{E}|_E := h_E \qquad (T \in \mathcal{T};\ E \in \mathcal{E}) \tag{14}$$

Given $\mathcal{T}$, $\mathcal{P}_k(\mathcal{T})$ denotes the linear space of $\mathcal{T}$-piecewise polynomials of degree $\leq k$

$$\mathcal{P}_k(\mathcal{T}) := \{ \gamma_h \in L^2(\Omega) : \forall T \in \mathcal{T},\ \gamma_h|_T \in \mathcal{P}_k(T) \} \tag{15}$$

where $\mathcal{P}_k(T)$ denotes the vector space of algebraic polynomials of total degree $\leq k$ regarded as mappings on the domain $T \subset \mathbb{R}^2$. Moreover let $\mathcal{B}_3(\mathcal{T})$ be the space of $\mathcal{T}$-piecewise cubic bubble functions.

$$\mathcal{B}_3(\mathcal{T}) := \{ u \in C(\Omega) : \forall T \in \mathcal{T}, u|_T \in \mathcal{P}_3 \text{ and } u = 0 \text{ on } \partial T \} \tag{16}$$

We restrict our numerical investigation to conform low order finite element schemes, i.e., constant approximation of shear variable γ. Following Arnold and Brezzi (Arnold and Brezzi, 1993) the finite element space (Figure 2a)

$$V_h \times W_h \times \Gamma_h := \left(\mathcal{P}_2(\mathcal{T}) \cap H^1_0(\Omega) \right) \times \left((\mathcal{P}_1(\mathcal{T}) \oplus \mathcal{B}_3(\mathcal{T})) \cap H^1_0(\Omega) \right)^2 \times \mathcal{P}_0(\mathcal{T})^2 \tag{17}$$

yield a stable discrete problem with unique solution $(\vartheta_h, w_h, \gamma_h)$. With the exact solution (ϑ, w, γ) and maximal mesh–size $h \to 0$ there holds

$$\| w - w_h \|_{H^1_0} + \| \vartheta - \vartheta_h \|_{H^1_0} + \| \gamma - \gamma_h \|_{H^{-1}(\mathrm{div}) \cap t \cdot L^2} \leq ch \left(\| w \|_{H^2} + \| \vartheta \|_{H^2} + \| \gamma \|_{H^1} \right) \tag{18}$$

The positive constant $c = c(\alpha, \Omega, k, c_\vartheta, ...)$ is independent of mesh size h and the plate's thickness t. Note, though (18) formulates strong restrictions on the continuous solution it yield only suboptimal, i.e., linear convergence. By a modification of parameter α, $\alpha = \alpha(\mathcal{T})$, Chapelle and Stenberg gained in (Chapelle and Stenberg, 1998) an improved a priori error estimation (cf. below).

Lovadina analyzed in (Lovadina, 1997) a finite element space (Figure 2b)

$$V_h \times W_h \times \Gamma_h := \left(\mathcal{P}_2(\mathcal{T}) \cap H_0^1(\Omega)\right) \times \left(\mathcal{P}_2(\mathcal{T}) \cap H_0^1(\Omega)\right)^2 \times \mathcal{P}_0(\mathcal{T})^2 \tag{19}$$

which leads to a stable scheme and quasi-optimal a priori error estimates in the sense that there exists a (h,t)-independent positive constant c such that

$$\begin{aligned} &\| \vartheta - \vartheta_h \|_{H_0^1(\Omega)} + \| w - w_h \|_{H_0^1(\Omega)} + \| \gamma - \gamma_h \|_{H^{-1}(\mathrm{div}) \cap t \cdot L^2} \\ &\quad \leq c\Big(\inf_{\phi_h \in V_h} \| \vartheta - \phi_h \|_{H_0^1(\Omega)} + \inf_{v_h \in W_h} \| w - v_h \|_{H_0^1(\Omega)} \quad + \quad \inf_{\eta_h \in \Gamma_h} \| \gamma - \eta_h \|_{H^{-1}(\mathrm{div}) \cap t \cdot L^2} \Big) \end{aligned} \tag{20}$$

In case of (19) and a smooth continuous solution, the poor approximation of the shear yields a convergence order $O(h)$ (Lovadina, 1997). Since the approximation errors of the remaining two best-approximation errors are of higher order, a subtle choice of the parameters α and β is expected to improve the convergence to $O(h^{3/2})$ due to (Boffi et al., 1997). We specify these effects in Section 3 and 4 and stress that, at least in the a posteriori error analysis, the constants α and $\beta = 1/(t^{-2} - \alpha)$ shall be monitored as well as t and h.

3 Stabilisation Technique

In a first numerical approach we apply the discretisations on a simple problem with known solution, calculated analytically in some characteristic points by Timoshenko and Woinowsky-Krieger (Timoshenko et al., 1987). A quadratic plate $(x,y) \in \Omega := [-0.5, 0.5]^2 m$ with thickness $t = 0.01m$ is all side clamped and uniformly loaded, $f = -1000N/m^2$, $E = 10.92 \cdot 10^6 N/mm^2$, $\nu = 0.3$. The maximal deflection is expected to be in the plate center. By symmetry we calculated only one quarter of the domain $[0, 0.5]^2 m$ with an uniform initial mesh $\mathcal{T}_1$ of 8 finite elements (4 squares, each divided into 2 triangles). Starting computation with this coarse mesh and $\alpha = 1$ as in (Arnold and Brezzi, 1993; Braess 1997) both finite element discretisations fail, the system shows spurious modes, Figure 1. (Note, in Figure 1 the whole plated domain is plotted and for displaying each finite element is divided into 4 triangles.) Only by refining (here with more than 2000 finite elements and $\alpha = 1$) we obtain correct approximation. Satisfying solution quality we compute with the coarse mesh $\mathcal{T}_1$ enlarging α by a factor of 10 ... 1000. Even larger numbers of α let the system become too stiff (cf. Weinberg, 1999).

Extensive numerical studies confirmed the discrete problem (12–13) to be asymptotically stable against α with $0 < \alpha < t^{-2}$, but preasymptotic performance as well as convergence rates strongly depend on it. Summarizing our experience we prosecute two strategies for choice of parameter α. First we adapt it to the finite element mesh size with $\alpha = O(h^{-2})$ due to (Weinberg, 1999; Chapelle and Stenberg, 1998), computing elementwise

$$\alpha = \alpha(T) = \frac{1}{h_T^2 + t^2} \tag{21}$$

Secondly, we choose a model dependent but fixed parameter α. Using a characteristic size of plate domain $l = l(\Omega)$ and plate thickness t, $l \gg t$, we employ

$$\alpha = \frac{1}{lt} \tag{22}$$

Both numerical rules, (21) and (22), imply $0 < \alpha < t^2$ and avoid spurious modes on coarse meshes. In the examples of this paper we set the characteristic plate size $l = 1m$.

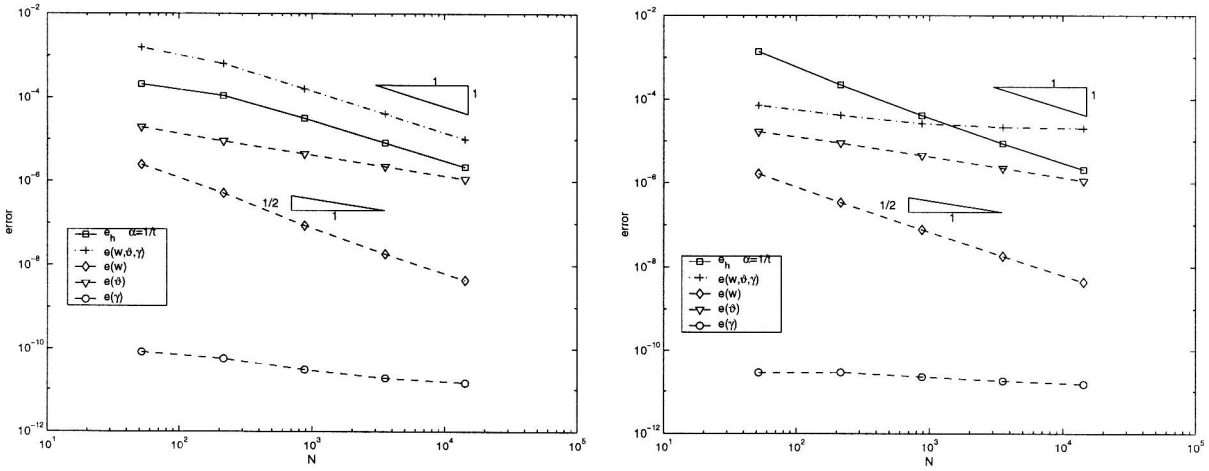

(a) $\alpha = 1/(lt)$ (b) $\alpha = 1/(h_T^2 + t^2)$

Figure 3: Quadratic plate: discretisation error with $P_2 - P_1^B - P_0$ fem

4 Global a posteriori Error Measure

The numerical validation of the theoretically predicted convergence rates requires comparisons with the unknown exact solution. But the design of a benchmark with known exact solution to (1)-(2) is difficult: if we prescribe a general vertical displacement w and rotations $\vartheta = (\vartheta_1, \vartheta_2)$ of the plate normal, this does not necessarily satisfy (1) (while we could choose f to satisfy (2)). Even more problematic is a *typical* choice of (w, ϑ), which reflects the finite element's performance in practice. One possible remedy is the relation to the Kirchhoff plate model

$$\frac{Et^3}{12(1-\nu^2)} \triangle\triangle w - f = 0 \tag{23}$$

as employed below. The main drawback is that the solution w of (23) is a good approximation to a solution of (1)–(2) only for very thin plates where Reißner–Mindlin's theory is not designed for. The remaining option is a model solution from a very fine finite element approximation with a reasonable method and mesh for further reference. Since mathematical results are usually provided for the error in energy (or equivalent) norms only it is not sufficient to compare a typical displacement or moment *at one* point of the domain. Hence, one needs the entire mesh and the nodal values from that mesh which is not easy to handle.

Thus we established in (Carstensen and Weinberg, 1999) a new method which allows an error representation in natural energy norm by one (problem depending) constant C and computable quantities known from (current) finite element solution. The constant C could be computed from f and the unknown w. But in practice we may use a finite element calculation on a very fine mesh or an extrapolation technique to provide this constant once for every problem. This enables a global a posteriori error estimation without any known solution. We will employ it below to assess approximation quality of different finite element schemes.

Here we start verifying the a priori error estimations of Section 2 under its strong assumptions (clamped boundaries, no singularities). We compute the quadratic plate from Section 3 with thickness $t = 0.001m$, but now we impose a load f enforcing the Kirchhoff solution

$$w(x,y) = (x - 1/2)^2(x + 1/2)^2(y - 1/2)^2(y + 1/2)^2 \tag{24}$$

We denote the H^1–norm of the difference between the Kirchhoff solution and the finite element solution for the displacement as well as for the rotation vector with

$$e(w) := \| w - w_h \|_{H_0^1(\Omega)} \quad \text{and} \quad e(\vartheta) := \| \vartheta - \vartheta_h \|_{H_0^1(\Omega)} \tag{25}$$

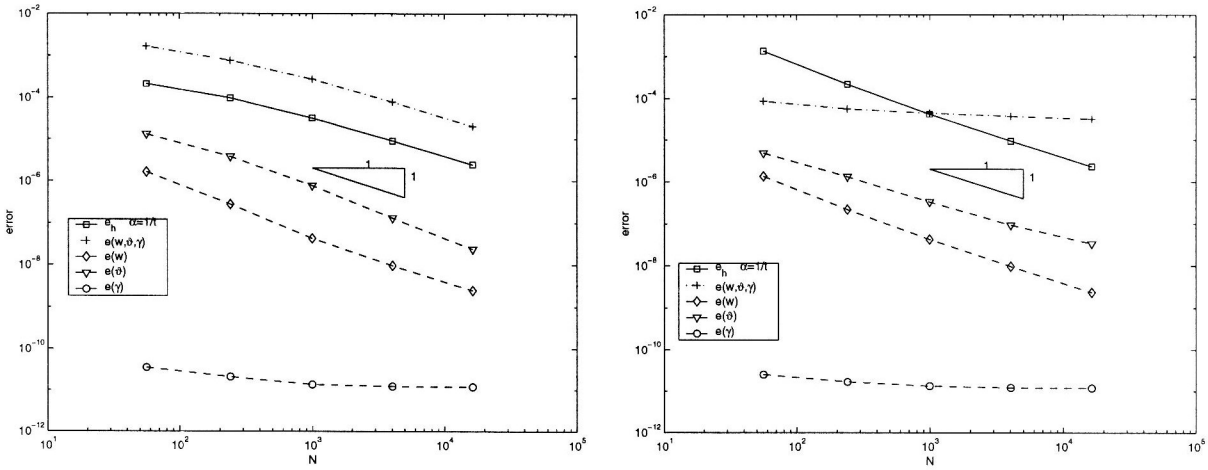

(a) $\alpha = 1/(lt)$ (b) $\alpha = 1/(h_{\mathcal{T}}^2 + t^2)$

Figure 4: Quadratic plate: discretisation error with $P_2 - P_2 - P_0$ fem

and analogous the shear error in L^2–Norm whereby the shear stress in the Kirchhoff theory is introduced by additional equilibrium conditions (Timoshenko, 1987)

$$e(\gamma) := \| \gamma - \gamma_h \|_{L^2(\Omega)} \tag{26}$$

The norm (11) is not computable and so it is estimated owing to an inverse estimate (Brenner and Scott, 1994) by

$$\| q \|_{H^{-1}(\Omega)} \leq c \| h_{\mathcal{T}} q \|_{L^2(\Omega)} \tag{27}$$

for $\mathcal{T}$-piecewise polynomials q. The estimate (27) is applicable here because the finite element solution and, as an exception, the analytical solution is a $\mathcal{T}$-piecewise polynomial. Ignoring constant c, we approximate the normed solution error

$$\| w - w_h \|_{H_0^1(\Omega)} + \| \vartheta - \vartheta_h \|_{H_0^1(\Omega)} + \| \gamma - \gamma_h + \alpha(\vartheta - \vartheta_h - \nabla(w - w_h)) \|_{H^{-1}(\mathrm{div}) \cap t \cdot L^2} \tag{28}$$

by

$$e(w, \vartheta, \gamma) := \big(e(w)^2 + e(\vartheta)^2 + (h_{\mathcal{T}}^2 + t^2) \| \gamma - \gamma_h + \alpha(\vartheta - \vartheta_h - \nabla(w - w_h)) \|_{L^2(\Omega)}^2 + h_{\mathcal{T}}^2 \| \mathrm{div}(\gamma - \gamma_h + \alpha(\vartheta - \vartheta_h - \nabla(w - w_h))) \|_{L^2(\Omega)}^2 \big)^{1/2} \tag{29}$$

Figure 3–4 display the error results from uniform mesh refinements and (a) for constant parameter α (resp. β) and (b) for mesh–adapted α in (3). (Here and below the error terms are plotted versus the number of degrees of freedom N in a log/log-scale; owing to $N \propto h^{-2}$ in two dimensions, a slope $-1/2$ in the figures corresponds to an experimental convergence rate 1. For comparisons, triangles with slopes $1/2$ and 1 are shown in the figures as well.) Single error contributions (dashed lines) show expected convergence rates (corresponding to V_h, W_h and Γ_h). But the approximation (29) (dashdotted lines) which in case (a) of constant α yield expected convergence rates of ≈ 1 fails in case of mesh adapted α (b). Our explanation for the poor convergence in case (b) is that the mesh-depending choice of α is not well-balanced with the strong norm of the physical shear-error. That norm (29) is not an opportune measure of discretisation error.

This is underlined by our observation of error convergence in natural energy norm (solid lines)

$$e_h := \big(\| C^{1/2} \varepsilon(\vartheta - \vartheta_h) \|^2 + t^{-2} \| \vartheta - \vartheta_h - \nabla(w - w_h) \|^2 \big)^{1/2} \tag{30}$$

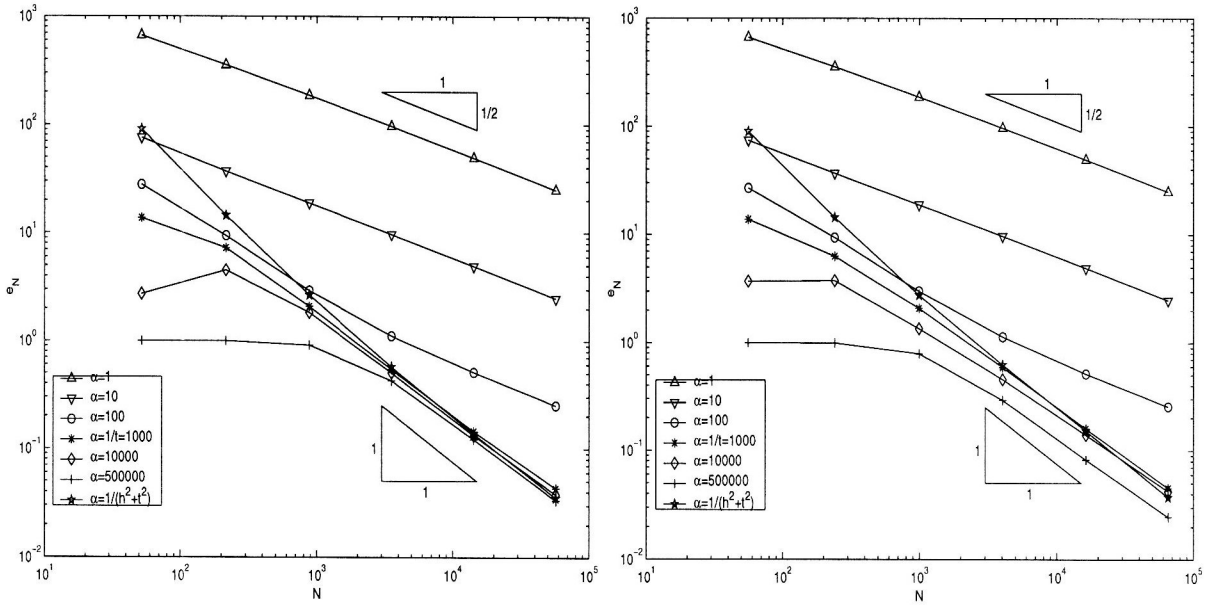

(a) $P_2 - P_1^B - P_0$ fem

(b) $P_2 - P_2 - P_0$ fem

Figure 5: Relative energy error for various α in the Example of Section 4

Hence, we apply the energy error to monitor the effect of parameter α in (12)–(13). From (Carstensen and Weinberg, 1999) we know that (30) equals the square root of

$$C - \| \mathcal{C}^{1/2}\varepsilon(\vartheta_h) \|^2 + t^{-2}\| \nabla w_h - \vartheta_h \|^2 - 2\big((t^{-2} - \alpha)(\nabla w_h - \vartheta_h) - \gamma_h; \nabla w_h - \vartheta_h\big) \tag{31}$$

with the real number $C := \big(f; w\big) = \| \mathcal{C}^{1/2}\varepsilon(\vartheta) \|^2 + t^{-2}\| \vartheta - \nabla w \|^2$. Given (24) we obtained $(f; w) = 2.3324 \cdot 10^{-10} Nm$ as an approximation to the unknown C.

In Figure 5 the relative error $e_N := e_h/\sqrt{C}$ is plotted for different values of α. We observe the predicted linear convergence for both discretisations (17) and (19) if α is a small number and a convergence rate of $3/2$ for $\alpha = 1/(lt)$. Even higher numbers of α show no convergence as long as the mesh is coarse. Hence, a mesh adapted α shows best convergence behaviour, an optimal convergence rate of 2 is obtained for both discretisations and $\alpha = 1/(h_T^2 + t^2)$.

5 Local a Posteriori Error Estimation and Adaptive Algorithm

The discrete problem is supposed to generate discrete solutions $(w_h, \vartheta_h, \gamma_h) \in H_0^1(\Omega)^2 \times H_0^1(\Omega) \times L^2(\Omega)$ which, as a minimal condition, satisfies (12)-(13) for all $(v_h, \phi_h, \eta_h) \in V_h \times W_h \times \Gamma_h$. Then, for each element $T \in \mathcal{T}$, we define our error indicator η_T by

$$\begin{aligned} \eta_T^2 \;&:=\; h_T^2 \int_T \Big(|f - \mathrm{div}(\gamma_h + \alpha(\vartheta_h - \nabla w_h))|^2 \\ &+\; |\gamma_h + \alpha(\vartheta_h - \nabla w_h) - \mathrm{div}\mathcal{C}\varepsilon(\vartheta_h)|^2 \Big) dx + h_T/t \int_T |\nabla \vartheta_h - D^2 w_h|^2 dx \\ &+\; \sum_{E \in \mathcal{E},\, E \subset \partial T} h_E \int_E \Big(|[\gamma_h + \alpha(\vartheta_h - \nabla w_h)] \cdot n_E|^2 + |[\mathcal{C}\varepsilon(\vartheta_h)] \cdot n_E|^2 \Big)\, ds \end{aligned} \tag{32}$$

Here, for a $\mathcal{T}$-piecewise continuous function, the square brackets $[\cdot]$ are defined as the jump over the edges: If $E = T_+ \cap T_-$ is a common edge of two distinct T_+ and T_- in $\mathcal{T}$ then, for $x \in E$, the jump $[G](x)$ is the limit of $G(x + \epsilon n_E) - G(x - \epsilon n_E)$ as $\epsilon \to 0^+$. Thereby $[G]$ is defined on the skeleton $\cup\mathcal{E} \setminus \partial\Omega$ of all inner boundaries of elements (its definition on the boundary $\partial\Omega$ has to be specified separately).

The local contributions η_T to the error estimator $\eta_{\mathcal{T}}$

$$\eta_{\mathcal{T}} := \left(\sum_{T \in \mathcal{T}} \eta_T^2 \right)^{1/2} \tag{33}$$

can be computed elementwise (once a discrete solution is known). With (32) we have a reliable a posteriori error estimate, i.e., (33) is an upper bound for the solution error measured with (28). The proof of reliability was given in (Carstensen and Weinberg, 2000), its result motivates the usage of the error indicators (32) for adaptive mesh refinement.

Adaptive Algorithm (A).

(a) Start with coarse mesh $\mathcal{T}_0$.

(b) Solve discrete problem with respect to $\mathcal{T}_k$ *with* N *degrees of freedom.*

(c) Compute η_T *for all* $T \in \mathcal{T}_k$.

(d) Compute error bound $\eta_N := \left(\sum_{T \in \mathcal{T}_k} \eta_T^2\right)^{1/2}$ *and terminate or go to (e).*

(e) Mark element T *red iff* $\eta_T \geq \frac{1}{2} \max_{T' \in \mathcal{T}_k} \eta_{T'}$.

(f) Red-green-blue-refinement to avoid hanging nodes, update mesh $\mathcal{T}_k$ *and go to (b).*

Red-green-blue-refinement means to split red–marked elements into four congruent elements. The neighboring, not marked elements are split in a way, that ever one longest side is divided. So we avoid hanging nodes as well as degenerated elements, Figure 6.

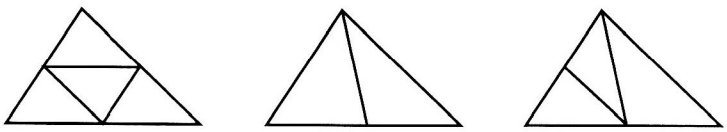

Figure 6: Red–green–blue refinement of a triangle

6 Numerical Examples for Practical Error Computation

6. 1 Sheet Metal with a Hole

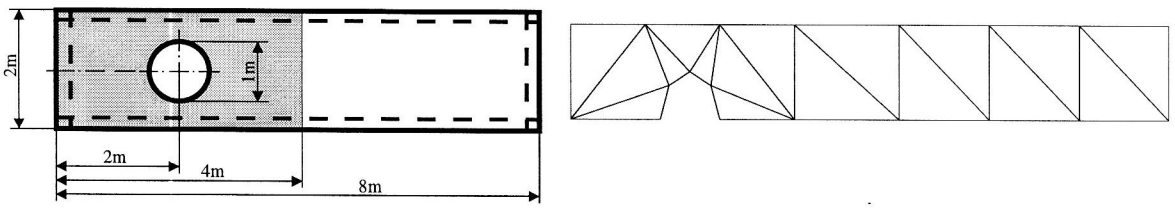

Figure 7: Sheet metal with hole and initial mesh

First, a rectangular sheet metal with a hole loaded by uniform pressure at half of the domain is computed, Figure 10, (f vanishes outside the marked region), $f = 10^6 N/m^2$, $E = 2.1 \cdot 10^{12} N/m^2$, $\nu = 0.3$, $t = 0.1m$. The plate is simply supported; we employ hard support (not only the displacements but also the tangential component of the rotations are forced to zero) to avoid boundary layer effects. By symmetry the coarse initial mesh consists of 17 finite elements, i.e., $N = 126$ or $N = 148$ degrees of freedom for $P_2 - P_1^B - P_0$ and $P_2 - P_2 - P_0$ discretisation, respectively.

The energy error is estimated with (31), an extrapolation technique yields $C = 2.444 \cdot 10^{-12} Nm$ (cf. (Carstensen and Weinberg, 1999) for details). The convergence of relative energy error e_N with uniform mesh refinement is plotted in Figure 8a. Despite of the hole the continuous solution is expected to be relatively smooth (no singular point). Hence we observe linear convergence rates of $P_2 - P_1^B - P_0$ and $P_2 - P_2 - P_0$–discretisation with a constant number of α (as theoretically predicted for clamped boundaries, (18), (20)). A mesh adapted α yields an improved convergence rate of about 2. There $P_2 - P_2 - P_0$ discretisation slightly better converges than $P_2 - P_1^B - P_0$ discretisation, but major influence of convergence rates has the choice of parameter α.

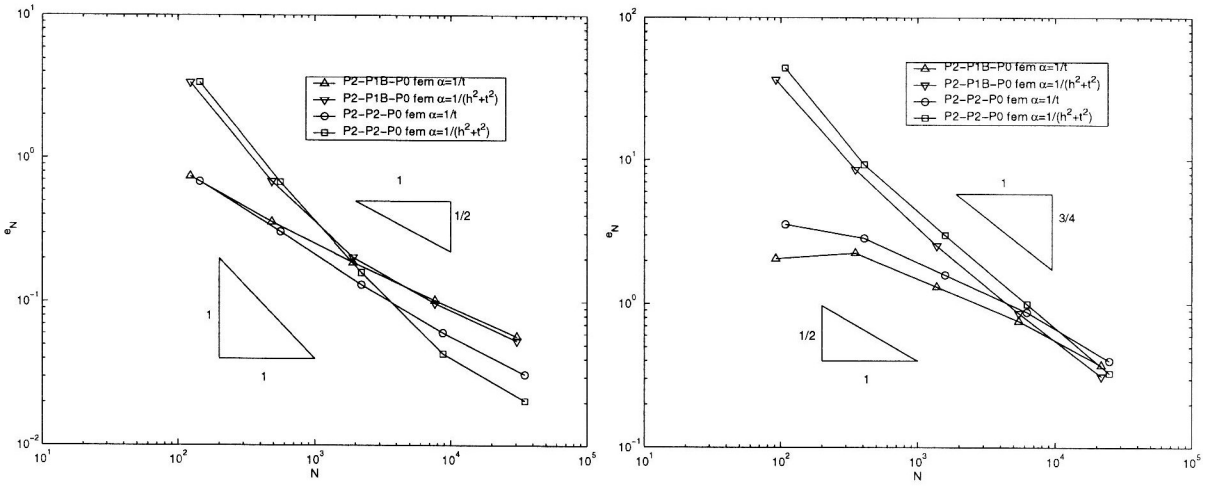

(a) Sheet metal with hole

(b) L–shaped domain

Figure 8: Relative energy error for different finite element schemes

6. 2 Solution Domain with re-entering Corner

In the second example an L-shaped plate $[-1,1]^2 \setminus (0,1)^2 m$ is clamped along the two edges of the domain which form the re-entering corner and is free at the remaining boundary. The (unknown) exact solution is expected to be singular near the origin at the re-entering corner even though the load is uniformly distributed; the material parameters are constant as in Section 3, $t = 0.01m$.

Figure 8b displays the relative energy error of the four finite element schemes, starting with coarse meshes (Figure 9a) and refining uniformly but presumably sub-optimal. Both finite element spaces (17) and (19) converge similar. Due to singularity the convergence rates are smaller than one if $\alpha = 1/(lt)$ but may be improved up to 3/2 in case of $\alpha = 1/(h_T^2 + t^2)$.

Reißner–Mindlin's model is designed for moderately thick plates, hence we compute now the energy error

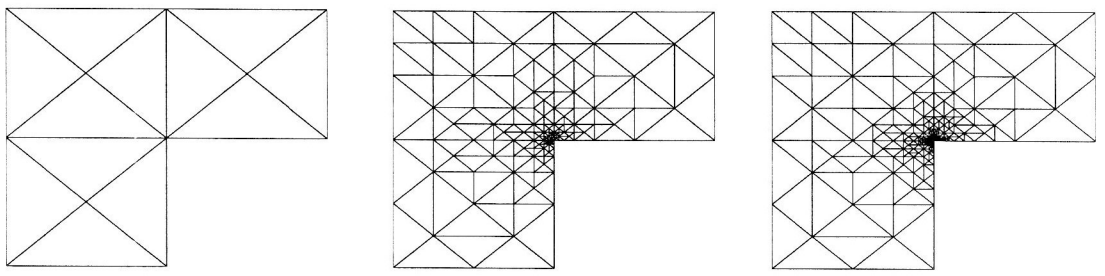

(a) Initial mesh $\mathcal{T}_0$

(b) Adaptive refined mesh $\mathcal{T}_5$

(c) Adaptive refined mesh $\mathcal{T}_7$

Figure 9: Finite element meshes in the example of Section 6.2

with different plate thickness $t = 0.1m, t = 0.01m$, and $t = 0.001m$, Figure 10 (extrapolated constant $C = 0.8366 \cdot 10^{-13} Nm$ if $t = 0.1$ and $C = 0.787 \cdot 10^{-19}/t^6 Nm$ else). Obviously thickness t has no significant influence on convergence rates, the discretisations are really locking free.

To assess the quality of error estimation for a non-uniform mesh, we employed the adaptive mesh-refining Algorithm (A) of Section 5. The initial mesh $\mathcal{T}_0$ and typical meshes $\mathcal{T}_5$, $\mathcal{T}_7$ after 5 and 7 refinement steps are shown in Figure 9 (here $t = 0.01, \alpha = 1/(h_T^2 + t^2)$). We obtain a significant reduction of error e_N up to convergence rate 2, Figure 10 (here displayed for $P_2 - P_2 - P_0$ discretisation only). The computation shows the expected superiority of adaptive refinement techniques.

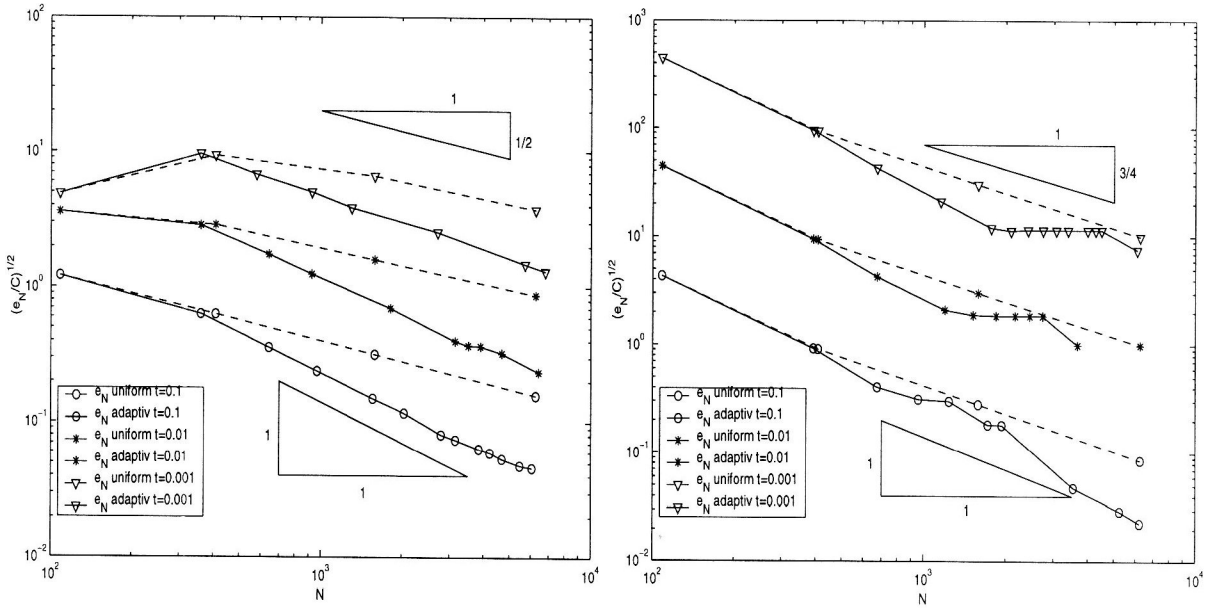

(a) $P_2 - P_2 - P_0$ fem, $\alpha = 1/(lt)$

(b) $P_2 - P_2 - P_0$ fem, $\alpha = 1/(h_T^2 + t^2)$

Figure 10: L–shaped domain: energy error (31) for uniform and adaptive mesh refinements

7 Approximation of Stress Resultants

7. 1 Example with Kirchhoff Solution

In engineering practice generally not the convergence rates of finite element methods are of interest but the computation of plate stresses and stress resultants (what, of course, strongly depends on each other). Thus we return to the example from Section 4 with analytical Kirchhoff solution (24) and monitor now the approximation of bending moments. The components of bending moment tensor m are associated with the continuous solution of (8)–(9) via partial derivatives (Timoshenko et al., 1987).

$$m := \frac{Et^3}{12(1+\nu)} \left(\varepsilon(\vartheta) + \frac{\nu}{1-\nu} \mathcal{I} \mathrm{tr} \varepsilon(\vartheta) \right) \tag{34}$$

Hence its approximation error is expected to be one order higher than the error of discrete solution $(w_h, \vartheta_h, \gamma_h)$. For the triangulation $\mathcal{T}$ of Ω let $\mathcal{K}_c$ be the set of all corner points, $\mathcal{K}_m$ denotes the set of all midpoints of the egdes $\mathcal{E}$, $\mathcal{K} := \mathcal{K}_c \cup \mathcal{K}_m$. With discrete solution $(w_h, \vartheta_h, \gamma_h) \in V_h \times W_h \times \Gamma_h$ the equations (34) yield discontinuous functions. Thus the finite element values referred to in Section 7 are mean values at $\mathcal{K}$, in the figures linked with straight dashed lines.

Computing one quarter $[0, 0.5]^2 m$ of the plate domain we evaluate the principle bending moments m_I, m_{II}, i.e., the eigenvalues of the bending moment tensor m, at $\mathcal{K}$ along a line from plate center C to one corner point A. The analytical Kirchhoff solution is plotted for comparison with solid lines, Figures 11–13. With the coarse mesh $\mathcal{T}_1$ we observe a rough approximation where only the $P_2 - P_2 - P_0$

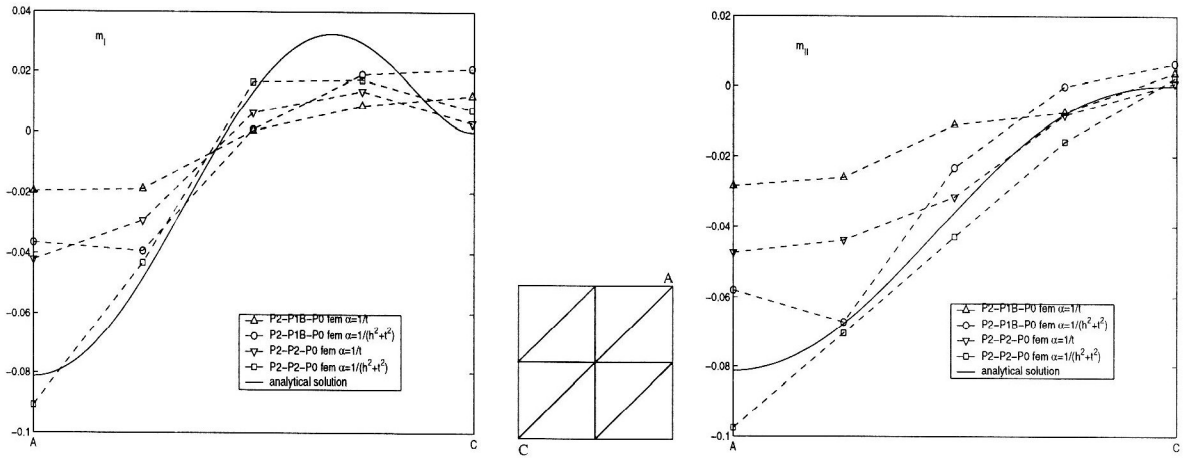

Figure 11: Principal bending moments m_I, m_{II} of Example 7.1, mesh $\mathcal{T}_1$

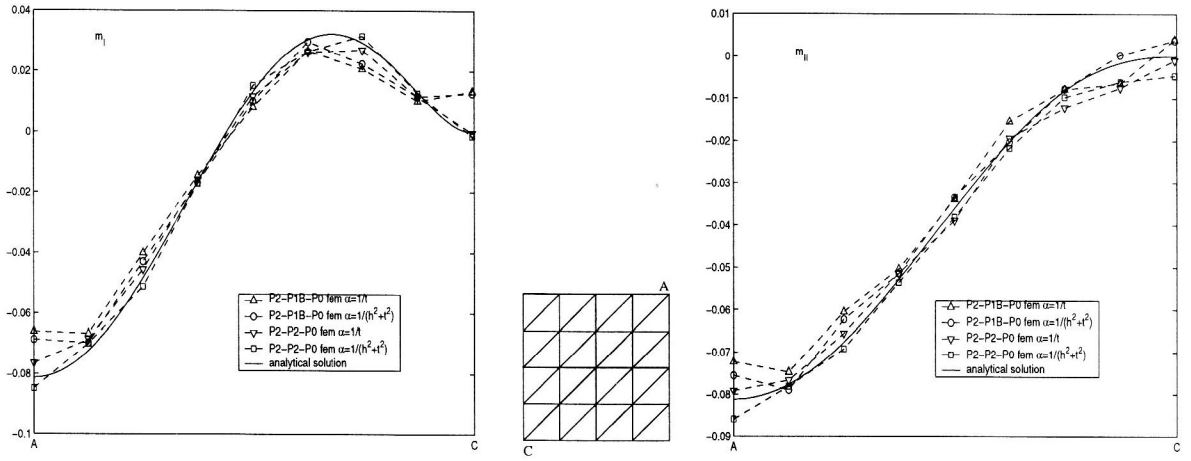

Figure 12: Principal bending moments m_I, m_{II} of Example 7.1, mesh $\mathcal{T}_2$

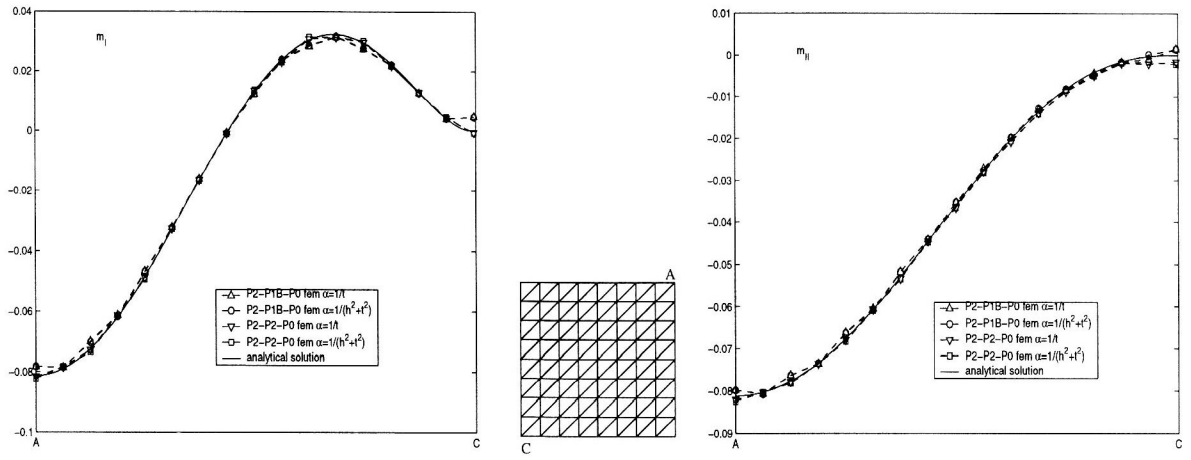

Figure 13: Principal bending moments m_I, m_{II} of Example 7.1, mesh $\mathcal{T}_3$

discretisation with mesh adapted α (21) yield qualitative correct elastic lines. After one step of uniform refinement (i.e., a finite element mesh $\mathcal{T}_2$ with 32 elements and approx. 200 degrees of freedom) already a satisfying approximation of bending moments is obtained. Again the $P_2 - P_2 - P_0$ discretisation with mesh adapted α yields best quality. This is confirmed in the next refinement step too, where its values lay completely on top of the analytical Kirchhoff solution. The results of mesh $\mathcal{T}_3$ (128 finite elements, approx. 1000 degrees of freedom) fit the analytical solution very well with all discretisations. From this practical point of view a further mesh refinement as done e.g. in Figure 7 is redundant.

The superiority of $P_2 - P_2 - P_0$ discretisation in computation of stress resultants (34) may not surprise. The discrete space for the rotations W_h contains P_2–functions in (19), whereas (17) approximates the rotations only by piecewise affine functions (though enriched with bubble functions).

7. 2 Benchmark with Stress Singularity

Finally we compute a rhombus plate with 60– and 120–degree angles, Figure 14. The plate of side length $s = 2m$ is all side hard simply supported and loaded uniformly with load $f = 10N/m^2$, $t = 40mm$ and material parameters of the example from Section 3. The skewed corners cause stress singularities at the obtuse angles.

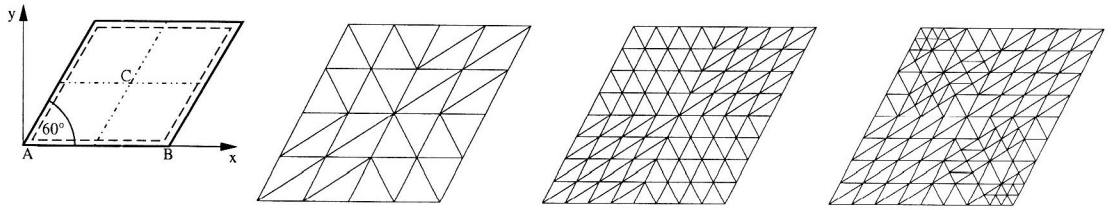

(a) (b) mesh $\mathcal{T}_2$ (c) mesh $\mathcal{T}_3$ (d) mesh $\mathcal{T}_3^a$

Figure 14: Benchmark rhombus plate, finite element meshes and adaptive refined mesh

Figures 15–16 display the principal moments m_I, m_{II} along a line from the 60–degree corner A to the plate center C to the 120–degree corner B. The plotted reference solution is obtained from a very fine $P_2 - P_2 - P_0$ discretisation T_6 (8192 elements, approx. 66000 degress of freedom), it coincides with a reference solution cited in (Stein et al., 1987). Morley (Morley, 1963) calculated an analytical solution based on (23) by expanding Fourier series at characteristic points. The values of our reference computation almost agree with (Morley, 1963), through slight differences might be caused by solving Reißner–Mindlin's formulation (8)–(9) instead of Kirchhoff theory in (Morley, 1963) but also by setting boundary conditions (here: hard simply support). The values in Table 1 (computed at the center of

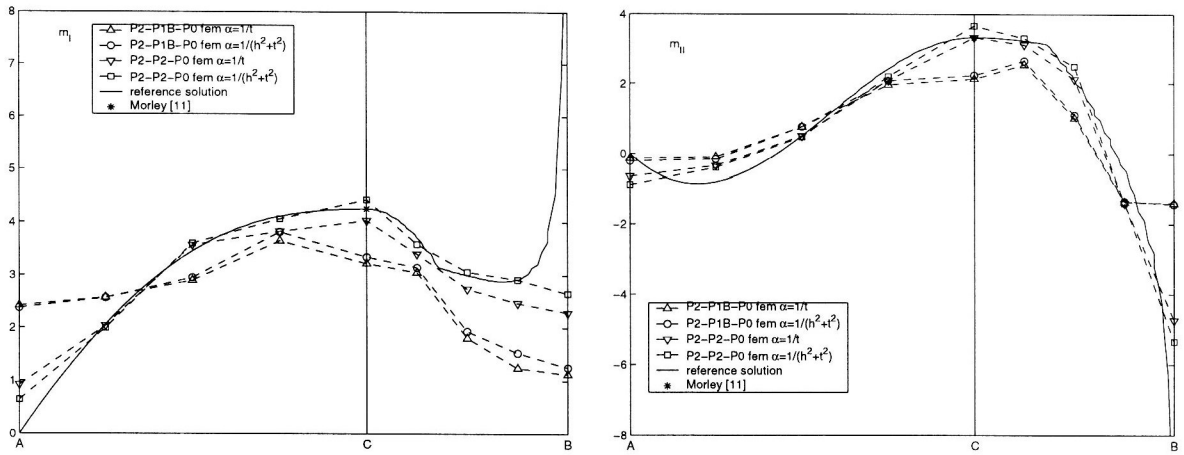

Figure 15: Rhombus plate: principal bending moments along A–C–B computed with mesh $\mathcal{T}_2$

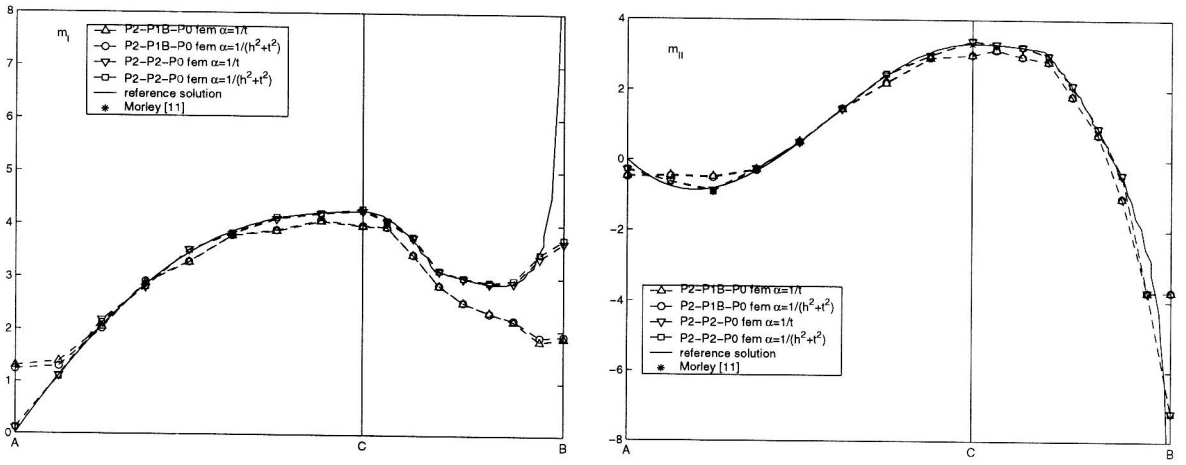

Figure 16: Rhombus plate: principal bending moments along A–C–B computed with mesh $\mathcal{T}_3$

the rhombus plate) as well as in Figure 15 and 16 are scaled, with $w := w \times 10^2 Et^3/(12f(1+\nu))$ and $m_{I/II} := m_{I/II}/(f \times s^2)$.

The bending moments computed with an initial mesh of 8 finite elements hardly corresponds with the reference solution. Figure 16 and 17 display the elastic lines obtained with meshes $\mathcal{T}_2$, $\mathcal{T}_3$ after 1 and 2 steps of uniform mesh refinement, respectively (32 resp. 128 finite elements). Again we observe a satisfying approximation of the stress resultants even with rather coarse finite element meshes and obtain best results applying the $P_2 - P_2 - P_0$ discretisation with mesh adapted α.

	mesh	w_C	m_{IC}	m_{IIC}
reference (Morley, 1963)		4.096	4.25	3.33
$P_2 - P_1^B - P_0$–fem, $\alpha = 1/(lt)$	$\mathcal{T}_1$	1.0342	0.7896	0.3881
	$\mathcal{T}_2$	3.1145	3.2170	2.1298
	$\mathcal{T}_3$	3.8291	3.9715	3.0045
$P_2 - P_1^B - P_0$–fem, $\alpha = 1/(h_\mathcal{T}^2 + t^2)$	$\mathcal{T}_1$	0	1.4135	0.7415
	$\mathcal{T}_2$	3.1546	3.3423	2.2356
	$\mathcal{T}_3$	3.8397	3.9859	3.0059
$P_2 - P_2 - P_0$–fem, $\alpha = 1/(lt)$	$\mathcal{T}_1$	2.1412	2.7205	1.8659
	$\mathcal{T}_2$	3.7701	4.0285	3.3232
	$\mathcal{T}_3$	4.0541	4.2584	3.4074
$P_2 - P_2 - P_0$–fem, $\alpha = 1/(h_\mathcal{T}^2 + t^2)$	$\mathcal{T}_1$	1.4135	5.1986	3.7781
	$\mathcal{T}_2$	3.8994	4.4235	3.6657
	$\mathcal{T}_3$	4.0653	4.2927	3.4130
	$\mathcal{T}_6$	4.0143	4.2530	3.3288

Table 1: Displacement w_C and bending moments m_{IC}, m_{IIC} in the center C of rhombus plate

Exemplarily Figure 14 displays a finite element mesh generated with Adaptive Algorithm (A) after 3 refinement steps, $\mathcal{T}_3^a$. Its computational effort is almost equal to uniform mesh $\mathcal{T}_3$ (1441 degrees of freedom, $P2-P2-P0$ discretisation) but we compute superior results, $w_C = 4.0760, m_{IC} = 4.2702, m_{IIC} = 3.4249$.

8 Conclusions

We illustrated the numerical performance of finite element schemes based on a modified mixed formulation of the Reißner–Mindlin equations. All presented schemes are locking free and — employing simple stabilisation techniques — stable in the preasymptotic range, too. The convergence rates of these schemes may be improved by a mesh adapted stabilisation parameter α and, additionally, by our automatic adaptive mesh refinement algorithm.

Summarizing we recommend a $P_2 - P_2 - P_0$ discretisation (19) with (21) for application in engineering practice. This finite element method yield optimal approximation quality.

Acknowledgements

The author thankfully acknowledges partial support by the German Research Foundation (DFG) within the Graduiertenkolleg 'Effiziente Algorithmen und Mehrskalenmethoden'.

Literature

1. Arnold, D. N.; Brezzi, F. F.: Some new elements for the Reissner-Mindlin plate model. Boundary Value Problems for Partial Differential Equations and Applications (J.L. Lions, C. Baiocchi, eds.) Masson, (1989), 287–292.
2. Arnold, D. N.; Falk R.S.: A uniformly accurate finite element method for the Reissner-Mindlin plate. SIAM J. Numer. Anal., 26, (1989), 1276–1290.
3. Boffi, D.; Lovadina, C.: Analysis of new augmented Lagrangian formulations for mixed finite element schemes. Numer. Math., 75, (1997), 405–419.
4. Braess, D.: Finite Elements. Cambridge University Press, (1997).
5. Brenner, S.C.; Scott, L.R.: The mathematical theory of finite element methods. Texts in Applied Mathematics, 15, Springer, (1994).
6. Brezzi, F.; Fortin, M.: Mixed and hybrid finite element methods. Springer, (1991).
7. Carstensen, C.; Weinberg, K.: Calculating the energy-norm FEM-error for Reissner-Mindlin plates without known reference solution. Mathematisches Seminar, Christian-Albrechts-Universität zu Kiel, Technical Report 00-03, (1999), (to appear in Comp. Mech).
8. Carstensen, C.; Weinberg, K.: Adaptive mixed finite element method for Reissner-Mindlin plates. Mathematisches Seminar, Christian-Albrechts-Universität zu Kiel, Technical Report 00-07, (2000), (subm. to CMAME).
9. Chapelle, D.; Stenberg, R.: An optimal low-order locking–free finite element method for Reissner–Mindlin plates. Math. Models and Methods in Appl. Science, 8, (1998), 407–430.
10. Lovadina, C.: A new class of finite elements for reissner-mindlin plates. SIAM J. Numer. Anal., 33, (1996), 2457–2467.
11. Morley, L. S. D.: Skew plates and structures. International Series of Monographs on Aeronautics and Astronautics. Pergamon Press, (1963).
12. Stein, E.; Lambertz, K.H.; Plank, L.; Reisch, A.: Element–Benchmark Rhombusplatte 60 grd. University Hannover, (1987).
13. Timoshenko, S. T.; Woinowsky-Krieger, S.: Theory of Plates and Shells. McGraw–Hill Book Company, (1987).
14. Weinberg, K.: An adaptive finite element approach for a mixed Reissner–Mindlin plate formulation. Mathematisches Seminar, Christian-Albrechts-Universität zu Kiel, Technical Report 22-99, (1999), (to appear in CMAME).

Address: Dr.-Ing. Kerstin Weinberg, Institut für Mathematik, Medizinische Universität zu Lübeck, Wallstr. 40, D-23560 Lübeck. *e-mail:* weinberg@math.mu-luebeck.de